NJC

Accepted Manuscript

This is an *Accepted Manuscript*, which has been through the Royal Society of Chemistry peer review process and has been accepted for publication.

Accepted Manuscripts are published online shortly after acceptance, before technical editing, formatting and proof reading. Using this free service, authors can make their results available to the community, in citable form, before we publish the edited article. We will replace this *Accepted Manuscript* with the edited and formatted *Advance Article* as soon as it is available.

You can find more information about *Accepted Manuscripts* in the Information for Authors.

Please note that technical editing may introduce minor changes to the text and/or graphics, which may alter content. The journal's standard Terms & Conditions and the Ethical guidelines still apply. In no event shall the Royal Society of Chemistry be held responsible for any errors or omissions in this *Accepted Manuscript* or any consequences arising from the use of any information it contains.

ROYAL SOCIETY OF CHEMISTRY

www.rsc.org/njc

Journal Name

RSCPublishing

ARTICLE

The effect of manganese in CdS/PbS colloidal quantum dot sensitized TiO_2 solar cell to enhance its efficiency

Cite this: DOI: 10.1039/x0xx00000x

Received 00th January 2012,
Accepted 00th January 2012

DOI: 10.1039/x0xx00000x

www.rsc.org/

Dinah Punnoose [a*], Hee-Je Kim [a], Hyun-Dong Lee [a], Challa Shesha Sai Pavan Kumar [b], Sunkara Srinivasa Rao[a], Sang- Hwa Chung[c]

Herein we demonstrate for the first time in exploring the impact of Mn on PbS and CdS distinctly using simple successive ion layer adsorption and reaction (SILAR) technique on TiO_2.The CdS passivation layer over PbS can reduce recombination of photo-injected electron with the electrolyte and enhance the overall performance and stability of the quantum dot sensitized solar cells (QDSSCs). The doping of Mn has a drastic impact on the host material (PbS/CdS) and can create new energy states that can delay the exciton recombination time and can allow charge separation. The surface roughness and morphology of PbS/Mn-CdS nanoparticles can be observed from atomic force microscopy images. The performances of the QDSSCs are examined in detail using polysulfide electrolyte with copper sulfide (CuS) counter electrode. Under the illumination of one sun (AM 1.5 G, 100 mW/cm^{-2}) the TiO_2/PbS/Mn-CdS QDSSCs exhibits power conversion efficiency (η) of 3.55%.

1. Introduction

Research on low dimensional systems has great advancements in understanding the effects of quantum confinement and its physical properties. [1-5] The quantum confinement allows the fine tuning of the optical properties and it is expected to favour efficient multiple exciton generation (MEG) [6-8] breaking the theoretical efficiencies of quantum dot solar cells (QDSSC) and is gaining more attention towards the development of next generation solar cells. The fabrication of QDSSC is analogous to that of dye sensitized solar cell (DSSC) which includes the deposition of narrow band gap semiconductors on mesoscopic TiO_2. [9] Upon excitation of nanostructured quantum dots (QD) the electrons are injected into TiO_2.The photo-current achieved from QDSSC are comparable with DSSC but the power conversion efficiencies are quite low due open circuit voltage and low fill factor. The I_3^-/I^- electrolyte used in DSSCs is not suitable for QDSSCs as it induces corrosion at the photo- electrode. [10, 11]

QDSSCs show a remarkable efficiencies and high photo-current in depleted hetero junctions [12] and also in Schottky configuration [13] with values of up to 7.3% and 5.2%. QDSSCs still shows limited efficiencies because of its charge recombination in the interface of the QDs. [14, 15] *In situ* growth methods have been widely used for the preparation of PbS, [16-18] CdS [19, 20] and CdSe [21, 22] QD-decorated photo-anodes. *In situ growth* techniques include chemical bath deposition (CBD) [23-26] and successive ionic layer adsorption and reaction (SILAR). [18, 27-28] QDs such as, CdS, CdSe, Bi_2S_3, PbS etc., [15, 16] have been reported as a potential photon sensitizer for QDSSCs. Lead sulfide (PbS) QDs shows a high absorption coefficient with tunable band gap of 0.41 eV, which is beneficial for efficient sensitizer for QDSSCs. [17] The quantized discrete band structures, the achievement of multiple exciton generation pushed PbS sensitized QDSSCs theoretical efficiency beyond the Shockley Queisser limit.[18] These encouraging properties open windows for research in exploring and developing the performance PbS based QDSSCs. Even though, several cycle of PbS sensitization shows an tremendous improvement in the short circuit current density (J_{SC}), but due to its back reaction of photo-injected

electrons with the electrolyte causes large drop in open circuit voltage (V_{OC}).

Braga *et al.* [17] reported that few passivation layers of CdS over the PbS sensitized surface of the photo-anode can reduce recombination of photo-injected electrons with the electrolyte and enhances the overall performance of the solar cells. Furthermore, increasing more than two cycles of PbS layers shows a drastic decrease in the performance of the QDSSCs with large drop in open circuit voltage of the cell. Owing to the partial passivation provided by the organic ligands, the dangling bonds remaining on the QD surface can perform as carrier trapping sites, which cut down the solar cell performance [29, 30].Inorganic materials such as CdS and ZnS are known to provide more complete passivation for the QD surface.[31] The ZnS SILAR coating technique has been used to protect QDs from photo corrosion and to suppress electron recombination with the electrolyte. [19, 25, 32]

In QDSSCs, the limitation is that, integration of QDs into the TiO_2 mesoporous matrix when attaining a good monolayer on the inner body of the TiO_2 electrode, which results in decreased efficiency. To overcome this, bilayer electrodes must be used, in which metal chalcogenides are sensitized with infrared dyes. Several approaches are used, such as crystal size control, introducing dopants, and optimizing the QD-sensitized electrode, its type, and the concentration of dopant, which could result in enhanced electrical and optical properties.[33-35] These properties can be enhanced by doping Mn^{2+}, Fe^{2+}, and Co^{2+} to QDs.

Of key importance in the exploration, the incorporation of Mn into PbS is an important methodology because it imparts paramagnetic properties.[36] Carrier-dopant exchange interactions occur in Mn doped PbS colloidal quantum dots, which indicates enhancements in both the valence and the conduction electrons. [37] Justin *et al.* worked on ZnO nano-rods with CdS/CdSe/ZnS and presented a promising passivation layer for PbS QDs. The open circuit potential (V_{OC}) is not affected, it defends against polysulfide electrolyte and the large accumulation of photo-injected electrons in the conduction band of the photo-anode by using this approach. This method lowers recombination of photoelectrons and increases the photovoltaic efficiency [38] but there is not an appreciated enhanced efficiency. Furthermore, ZnO has the disadvantage of which it is susceptible to dissolution processes during the heterogeneous photo-catalytic process. Henceforth we are using TiO_2 semiconductor which is frequently used because of its good chemical and photochemical stability, it exhibits high photo-catalytic activity, is non-toxic and is abundant and cheap decorated photo-anodes.

The work of Kamat *et al.* on Mn-doped CdS photo-anode opens windows for research in exploring new methodologies in achieving a high photovoltaic performance in QDSSCs Under standard simulated AM 1.5 G (100 mW/cm^2) illumination, a solar-cell-based CdS QD-sensitized TiO_2 electrode can present a power conversion efficiency of 1.93%.[39] Most importantly, by exchanging CdS with an Mn-CdS shell, the conversion efficiency of Mn-CdS QDSSCs has been further improved to 2.53%, which is one of the best results for CdS-based QDSSCs. Recently, Yu *et al*. reported that the Mn-doped CdS QDSSCs achieved conversion efficiency of 1.19% [40] Such results motivated us to explore the Mn doped CdS quantum dots to improve photovoltaic performance in QDSSCs. On the other hand, to the best of our knowledge, no efficient study is performed in understanding the influence of manganese in PbS and CdS colloidal quantum dots distinctly. One of the main reasons for enhanced photovoltaic properties is because of the combination of successive layers of PbS which has better light harvesting ability and makes large accumulation of photo-injected electrons in the conduction band of TiO_2. The other is, the Mn impurities have a drastic impact on the host material and can create new energy states that can delay the exciton recombination time and can allow charge separation. The PbS QDs with paramagnetic and optical properties can be tunable by the Mn content.

We fabricated CdS, PbS/CdS, Mn-PbS/CdS, PbS/Mn-CdS co-sensitized TiO_2 for QDSSCs. Polysulfide electrolyte and a CuS counter electrode were used, as shown in Figure 1.Doping Mn with both CdS and PbS QDs distinctly was done to reduce the recombination reactions in the TiO_2 system. Due to the increase in QD deposition and reduced electron recombination, QDSSCs based on the PbS/Mn-CdS showed a significant increase in power conversion efficiency of 3.55%, which is higher than that of CdS-sensitized bare TiO_2.

Journal Name RSCPublishing

ARTICLE

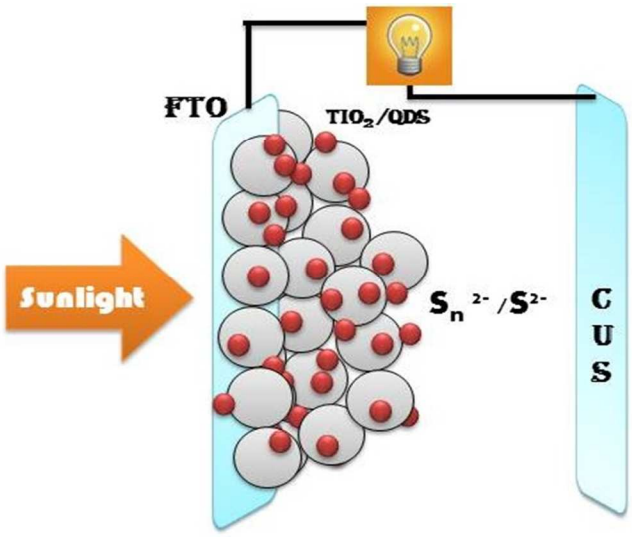

Figure 1. Graphical representation of CdS, PbS/CdS, Mn-PbS/CdS, PbS/Mn-CdS on QDSSCS with CuS counter electrode and polysulfide electrolyte and its details.

2. Experimental Section

2.1 Materials

All chemicals used were purchased from Aldrich and employed without any further purification. FTO substrate with a sheet resistance of 10Ω/square (Sigma-Aldrich) was used to prepare photo-anodes and CE.TiO_2 paste(Ti-Nanoxide HT/SP) were supplied by Solaronix.

2.2 Fabrication of TiO_2 and CdS, PbS/CdS, Mn-PbS/CdS, PbS/Mn-CdS electrodes

With the aim of preparing QDSSCs the fluorine-doped tin oxide glass (FTO) is used as the substrates for both the photo-anode and CE. TiO_2 photo-anodes were fabricated on ultrasonically well-cleaned FTO substrate using the doctor blade method. Anatase TiO2 particles (Ti-Nanoxide HT/SP, Solaronix) are first deposited on the FTO substrates with an active area of 0.27 cm^2, followed by sintering at 450 °C for about 30 min. A thickness of ~7 µm is obtained. The prepared TiO_2 electrodes were used for further sensitized with CdS, PbS/CdS, Mn-PbS/CdS and PbS/Mn-CdS.The CdS QDs were sensitized on TiO_2 using the SILAR technique [18, 27-28]. The TiO_2 photo-anodes were immersed in a solution containing CdS 0.1 M cadmium acetate dehydrate solution for 5 minutes to allow Cd^{2+} ions to adsorb, and then it is rinsed with DI water and ethanol to remove the excess Cd^{2+} ions and in 0.1 M Na_2S for 5 minutes, where the pre-adsorbed Cd^{2+} ions react with S^{2-} ions to form CdS. Then, the electrodes were rinsed with DI water and ethanol and dried under N_2 gas. These two dipping procedures constitute one cycle, and five cycles were applied.

The TiO_2 photo-anodes were immersed in a solution containing 25 mM $Pb(NO_3)_2$ for 5 minutes to allow Pb^{2+} ions to adsorb, and then it is rinsed with DI water and ethanol to remove the excess Pb^{2+} ions. Photo-anodes were then dipped into an aqueous solution containing 0.1 M sodium sulfide (Na_2S) for 5 minutes, where the pre-adsorbed Pb^{2+} ions react with S^{2-} ions to form PbS. Then, the electrodes were rinsed with DI water and ethanol and dried under N_2 gas. These two dipping procedures constitute one cycle, and two cycles were applied. Then, CdS is sensitized for five cycles using an aqueous solution of 0.1 M cadmium acetate dihydrate and 0.1 M Na_2S to achieve good adsorption over the PbS/TiO_2 photo-anode. Figure 2 shows a schematic diagram of fabrication process of TiO_2 photo-anodes and CdS, PbS/CdS, Mn-PbS/CdS and PbS/Mn-CdS electrodes.

For the doping of Mn^{2+} to PbS, Mn $(CH_3COO)_2{\cdot}4H_2O$ were mixed with the $Pb(NO_3)_2$ to enable the co-adsorption of Mn^{2+} and Pb^{2+} ions. For the doping of Mn^{2+} to CdS, Mn $(CH_3COO)_2{\cdot}4H_2O$ were mixed with the cadmium acetate dehydrate to enable the co-adsorption of Mn^{2+} and Cd^{2+} ions. Finally, two cycles of ZnS passivizing layers were coated over CdS, CdS/PbS and CdS/Mn-PbS and Mn-CdS/PbS sensitized photo-anodes by the SILAR method using an aqueous solution of 0.1 M Zn $(NO_3)_2$ and 0.1 M (Na_2S), and each is dipped for 5 min per cycle and washed several times, dried, and used for the fabrication of QDSSCs. The ZnS can proficiently cover the bare TiO_2 and QDs, resulting in

strong inhibition of the electron leakage from either the QDs or TiO_2 to the electrolyte.

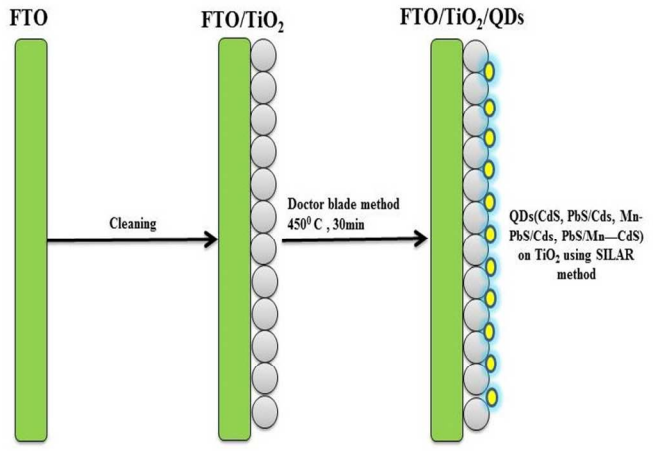

Figure 2. Fabrication process of TiO_2 photo-anodes and CdS, PbS/CdS, Mn-PbS/CdS and PbS/Mn-CdS electrodes.

2.3 Fabrication of a counter electrode

CBD is a modest and easy method for preparing the metal sulfide CE and FTO substrate. Prior to deposition, the FTO samples were cleaned ultrasonically using acetone, ethanol, and DI water for 10 minutes each. The prepared substrates were dried with N_2 gas. A CuS aqueous solution is prepared using 0.1 M $CuSO_4.5H_2O$ and 0.4 M $Na_2S_2O_3$ as sources of Cu^{2+} and S^{2-} ions. 0.4 M CH_4N_2O is used as a reagent for depositing CuS thin films. The substrates were then dipped horizontally into the solutions of CuS and kept in a hot air oven at 65 °C for about 2 h. The CuS-coated films were washed several times with DI water and ethanol.

2.4 Assembly of QDSSCS

The CdS, PbS/CdS, Mn-PbS/CdS and PbS/Mn-CdS QD-sensitized TiO_2 electrode and the CuS CE were assembled and sealed in layers using a transparent 50-μm hot melt sealing sheet (double sheet of SX 1170-25, Solaronix). Polysulfide electrolyte is injected through a pin-hole made in the CE. The cells were left for a few hours to complete the diffusion of electrolyte within the photo-anode, and the cells were tested under one sun illumination (AM 1.5 G, 100 mW/cm^2).

2.5 Characterizations

The surface morphology of the thin films were characterized using a field emission scanning electron microscope (FE-SEM, S-4200, Hitachi) equipped with energy dispersive X-ray spectroscopy (EDS) at an operating voltage of 15 kV to determine the elemental composition. QD adsorption is measured by UV-Vis spectroscopy (Mecasys, OPTIZEN 3220UV) over the wavelength range of 300-800 nm. The current-voltage characteristics of the QDSSCs were investigated under 1 sun illumination (AM 1.5G, 100 mW cm^{-2}) using an ABET Technologies (USA) solar simulator. The surface roughness of the substrates prepared using SILAR is characterized by atomic force microscope (JPK NanoWizard II AFM, JPK instruments, 158 Berlin, Germany) with a scan rate of 0.8 Hz in contact mode. Electrochemical impedance spectroscopy (EIS) is also used on the QDSSCs with CuS CEs using a BioLogic potentiostat/galvanostat/EIS analyzer (SP-150, France) under 1 sun illumination. The frequency ranged from 100 mHz to 500 kHz.

3. Results and Discussion

The QDs were synthesized by adapting to the reported procedures. [18, 27-28] An illustrative scheme of the QDs is shown in Figure 3.The formation of the Mn-CdS on PbS induces a notable enhancement of the photoluminescence properties of the QDs due to an efficient surface defect passivation.

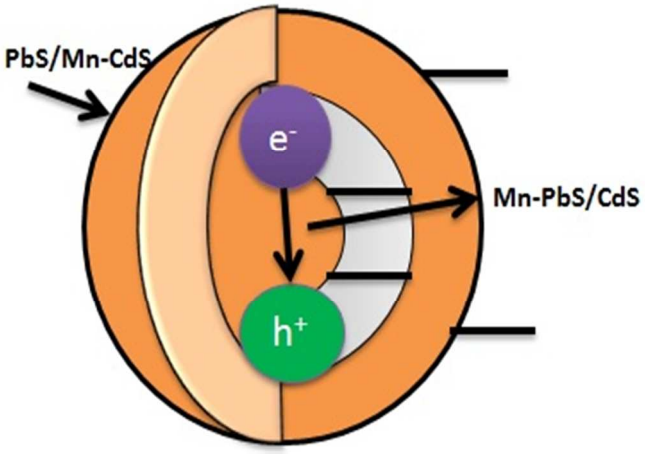

Figure 3 . Schematic structure and relative energy levels of the QDs.

3.1 Surface Morphology

Scanning electron micrograph (SEM) which reveals the surface morphology of bare CdS, PbS/CdS and Mn-PbS/CdS, PbS/Mn-CdS on TiO_2 is shown in Figure 4. The bare CdS electrode has a nano round shaped like structured and thus concentrates a high surface area with uniform distribution on the TiO_2 surface in Figure 4 (a). When CdS was passivized on PbS the surface becomes closer than bare CdS QDs as shown in Figure 4 (b).The gaps between the nano round shaped QDs were reduced by incorporating Mn to PbS/CdS shown in Figure 4(c).This methodology produces well dispersed round-shaped QDs with good size uniformity.The PbS/Mn-CdS describes a permeable inland with a large number of nano round shaped QDs (Figure 4(d)) due to which there could be a better photovoltaic performance because there are still less number of gaps is observed when Mn was incorporated to CdS when compared with Mn-PbS/CdS.

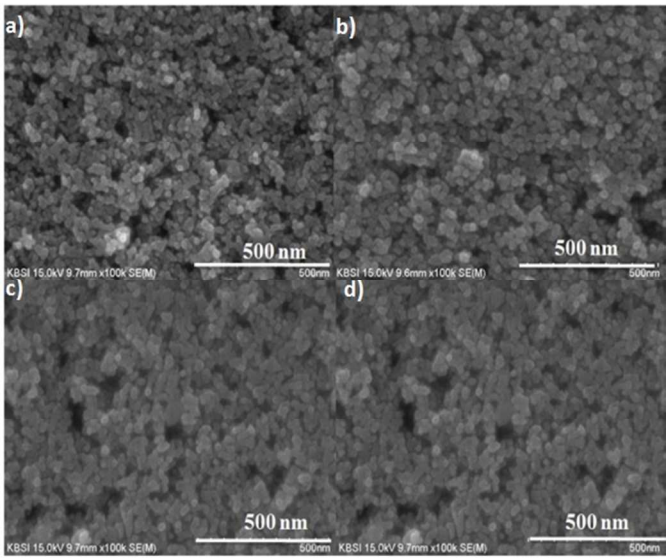

Figure 4. SEM images of (a) CdS (b) PbS/CdS (c)Mn-PbS/CdS (d)PbS/Mn-CdS sensitized electrodes on the surface of TiO_2.

The recombination decreases which is attributed by doping Mn that leads to the increase in the efficiency. The amount of adhesion of the active materials on FTO is the vital factor in determining the efficiency of the QDSSCs. If the materials do not stick to the FTO, they may be peeled off from the FTO substrate and released into the electrolyte, thus decreasing the efficiency of the QDSSCs [41]. Accordingly, the efficiency of the QDSSCs is enriched by refining the surface morphology of the electrode from compact to the porous together with particle ornamented surface architecture.

In order to confirm the crystal structure, and phase purity of as obtained thin films are examined using XRD analysis. The XRD analysis was measured for bare CdS, PbS/CdS and Mn-PbS/CdS and PbS/Mn-CdS films on TiO_2 which is shown in Figure 5. The sensitized films were dried in air and examined without calcinations. The detailed observations are shown in Table 1. All of the diffraction peaks well matches with the standard XRD pattern obtained through the prepared process. The diffraction peaks matches with the observed diffraction peaks. However, the XRD pattern of the films could not exhibit any characteristic peaks, which might be due to very thin thickness of the materials to be analysed and/or due to the interference of the XRD signals from the high crystallinity of the FTO substrate. In general, it is reported that the wet deposited composite films are amorphous and/or nano crystalline. [42]

Table 1 The detailed XRD analysis of PbS/CdS/ZnS thin fil

S.NO	Name	2θ(degrees)	JCPDScard no and its corresponding planes
1	TiO_2	25.272, 37.799, 48.049, 53.331	001-084-1286 [1 0 1] [0 0 4] [2 0 0] [1 0 5]
2	PbS	30.069,43.08, 62,521	05-0592 [2 0 0] [2 2 0] [4 0 0]
3	CdS	30.737, 44.039, 54.669	01-080-0019 [2 0 0] [2 2 0] [4 0 0]
4	ZnS	33.676, 47.739, 57.641,73.055	00-039-1363 [1 0 5] [1 1 0] [2 0 4][2 2 0]

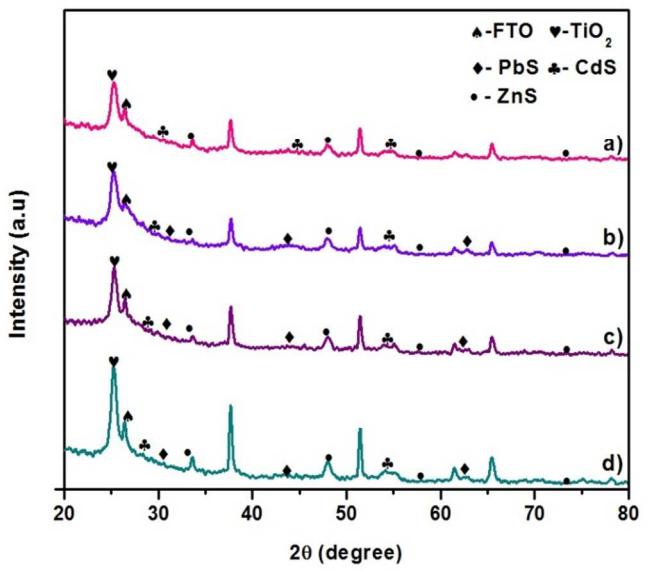

Figure 5. XRD pattern of (a) CdS (b) PbS/CdS (c)Mn-PbS/CdS (d)PbS/Mn-CdS sensitized electrodes on the surface of TiO_2.

To study the surface roughness of CdS, PbS/CdS, Mn-PbS/CdS, PbS/Mn-CdSfilms, high-resolution tapping-mode atomic force microscopy (AFM) was applied, and the corresponding 2-dimensional (2D) and3-dimensional (3D) images are shown in Figure 6.

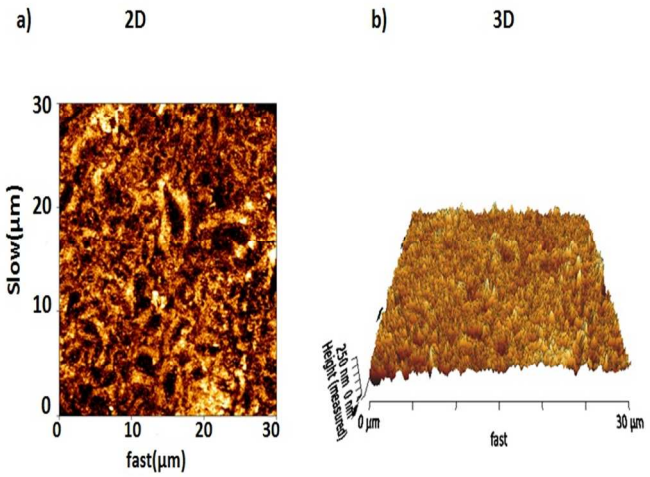

Figure 6. 2D (a, b) and 3D AFM images of PbS/Mn-CdS sensitized electrodes on the surface of TiO_2.

The smoothest film, with a root-mean square (RMS) roughness value 23.46nm was from the PbS/Mn-CdS electrode. The lower surface roughness is mainly due to the large particle sizes of PbS/Mn-CdS as compared with CdS, PbS/CdS, Mn-PbS/CdS nanostructures which might due to the lesser radii of Mn than Cd. Thus, during the deposition of PbS/Mn-CdS by SILAR, some of Mn ions are easily substituted by Mn-ion into CdS nanostructures. The power conversion efficiency of the CdS, PbS/CdS, Mn-PbS/CdS solar cell mainly depends on the small roughness of the surface, and a reduction of the surface roughness in PbS/Mn-CdS tends to improve the conversion efficiency of the QDSSCs, which affects the optical properties. [43]

3.2 Optical properties

The UV-Vis absorption of each substrate according to the deposited material is shown in Figure 7. The absorption edge of the TiO_2 photo-anode appears at about 360 nm. The absorption of the bare CdS photo-anode is near 500 nm, and the absorption of other substrates shifted towards longer wavelengths. The intensity of the absorbance is higher for the Pbs/Mn-CdS than for the bare CdS, PbS/CdS photo-anode and Mn-PbS/CdS. This indicates that the addition of manganese to the Pbs/Mn-CdS QDs can improve the light harvesting ability of the photo-anode because of PbS and more over there is an increase in absorption intensity after Mn^{2+} doping to CdS.

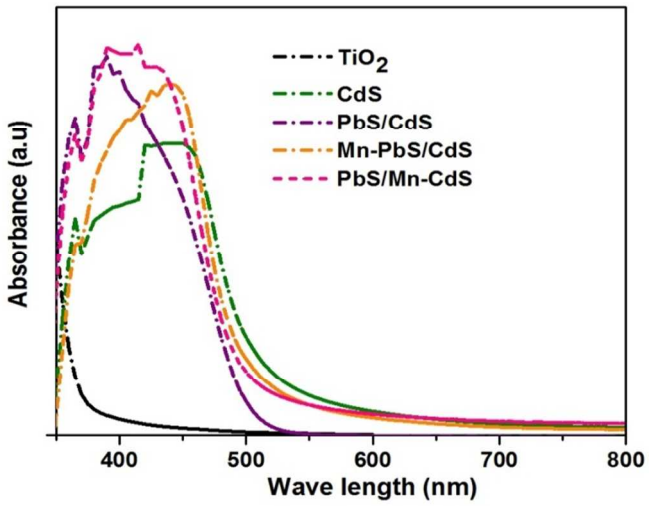

Figure 7. UV- vis absorption spectra of CdS, PbS/CdS, Mn-PbS/CdS and PbS/Mn-CdS sensitized electrodes on the surface of TiO_2.

This was attributed to the 3d-orbital energy level splitting of Mn^{2+}, which can be generally observed in transition metal complexes. Next, Mn-PbS/CdS second highest absorption which could be due to the slightly broader size distribution in the doped sample or the incorporation of Mn ions into the crystal lattice of PbS. The longer wavelength response of PbS/ Mn-CdS parallels the behavior seen in the absorption spectra. Generally in PbS sensitized solar cells, the

low band gap of bulk PbS (0.41 eV) shows an inability of electron transfer to the conduction band of the semiconductor photo-anode i.e., the conduction band position of PbS is much lower than that of semiconductor. But in case of PbS quantum confinement the conduction band of PbS tend to an upshift, allowing the fast electron into the semiconductor photo-anode. [44,45,46] Apart from this the consecutive CdS passivation layers over PbS can also favour more stability against the polysulfide electrolyte.

Even though the conduction band alignment shows an excellent electron transfer, but the valence band shows slight variation (i.e. the valence band of Mn- CdS is lower than the PbS) which can seriously affect the overall performance of the cell due to inefficient hole transfer. This might be the reason for the existence of low fill factor and efficiency than the expected overall performance of the QDSSCs. [47] The device stability is found to depend more on the interface and band alignment between the QDs and anodes rather than on the bulk QD layer itself. The band gap of PbS (1.56 eV), and CdS (2.54 eV) is obtained from the absorption spectrum and it is higher than that of bulk by the indication of the quantum confinement effect.

3.3 Photovoltaic properties

The ultimate performances of the devices have been studied.The deposition of the CdS, PbS/CdS, Mn-PbS/CdS and PbS/Mn-CdS on the TiO_2 surface were conducted.The cells were fabricated using FTO/TiO_2/CdS, PbS/CdS, Mn-PbS/CdS, PbS/Mn-CdS and a polysulfide electrolyte as the hole transporter. The photocurrent of the electrodes changes indicating that the Mn incorporation affects the absorbance of visible light and induces a higher current density. This also shows that Mn must be doped in the PbS/CdS distinctly. The J-V curves of CdS, PbS/CdS, Mn-PbS/CdS, PbS/Mn-CdS cells under one full sun (100 mW/cm^2) are shown in Figure 8. Photovoltaic parameters like open circuit voltage (V_{OC}), short circuit current (J_{SC}), fill factor (FF), and total energy conversion efficiency (η) are listed in Table 2. However, an increase in the V_{OC} is seen in PbS/Mn-CdS (0.56) and Mn-PbS/CdS (0.51).

Similarly, Mn-doped films also exhibited significant increase in the J_{SC} as compared to the corresponding semiconductor films without dopants. The fill factor remained almost the same for all four QDSSCS, implying similar electrochemical limitations during conversion of light into electricity. The increase seen in the J_{SC} and the V_{OC} with Mn doped system is reflected in the overall power conversion efficiency. The efficiency of 3.55% is obtained with PbS/Mn-CdS film is one of the highest performing QDSSCs. The current density (J_{SC}) of PbS sensitized cell shows a higher order of increase from 9.8 to 12.9 mA cm^2. This increase in current density is responsible for the enhancement of conversion efficiency. This is due to the positive influence of PbS QDs in overall performance of QDSSCs by enhancing the photoelectrons harvesting efficiency of the photo -anode.

Table 2 The Summary of the photovoltaic properties of CdS, PbS/CdS, Mn-PbS/CdS, PbS/Mn-CdS with CuS counter electrode.

Parameter	CdS	PbS/CdS	Mn-PbS/CdS	PbS/Mn-CdS
V_{OC}	0.49	0.50	0.51	0.56
J_{SC}(mA cm-^{2})	7.4	9.8	11.38	12.9
FF	0.52	0.52	0.54	0.49
η(%)	1.93	2.46	3.06	3.55

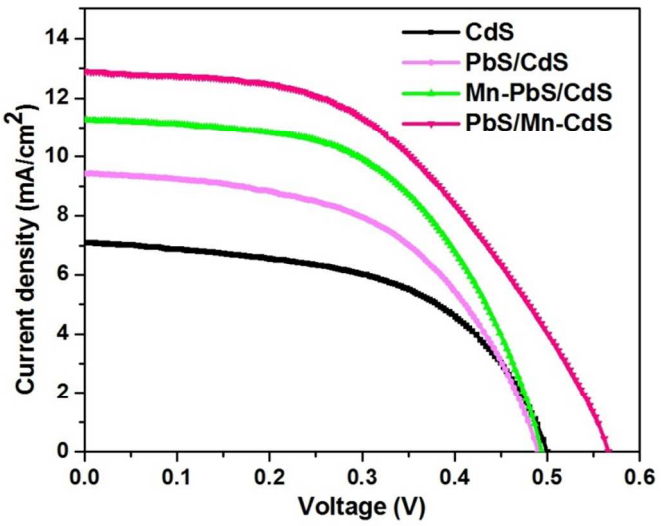

Figure 8. The photocurrent density-voltage curves of CdS, PbS/CdS, Mn-PbS/CdS, PbS/Mn-CdS with CuS counter electrode.

The enhancement in the photo electrochemical performance seen with quantum dot sensitization of TiO_2 is another milestone for

achieving greater efficiencies. This confirms the presence of Mn-CdS passivation layer over PbS photo-anode have considerably increased the stability of the PbS QDs in the photo-anode. The main reason is for enhanced photovoltaic properties is that the Mn impurities have a drastic impact on the host material and can create new energy states that can delay the exciton recombination time and can allow charge separation. V_{OC} can be calculated using the potential difference between the Fermi energy levels near the conduction band edge and the redox potential of the electrolyte. Consequently, the pre-treated interfacial doped buffer layers can help the electron accumulation inside the TiO_2 photo-anode. The doping of CdS films with Mn has enabled us to achieve a significant improvement as compared to undoped films.

3.4 Electrochemical impedance studies

Electrochemical impedance spectroscopy (EIS) is a powerful tool for characterizing the performance of each component of QDSSCs, and it is used to investigate the interior resistance, recombination, and charge transfer kinetics of QDSSCs. The Nyquist plots of QDSSCs with CdS, PbS/CdS, Mn-PbS/CdS, PbS/Mn-CdS photo-anodes were measured under a simulated light source. The equivalent circuit diagram model (inset of Figure 9.) consists of, the series resistance (R_S) is the non-zero intercept on the real axis of the plot. It represents the sheet resistance of the transparent conducting film (TCO) and the resistance of the FTO/TiO_2. The electron transfer resistance (R_{CT}) is associated with electron recombination at the photo-anode/electrolyte interface, and it is parallel with the chemical capacitance (Cμ). The finite Warburg impedance (Z_d) elements are associated with diffusion processes, which are influenced by the behaviour of the porous electrode/electrolyte interface and the counter electrode/ electrolyte. Z_d in the lowest frequency region is because of the Warburg impedance of the redox couple in the electrolyte. [48] The R_{CE} and C_{CE} are related to counter electrode resistance and capacitance.

To understand the carrier transport dynamics in these devices the parameters are determined. The parameters obtained from the EIS analysis are shown in Table 3. Figure 9 shows the Nyquist plots of QDSSCS fabricated using CdS, PbS/CdS, Mn-PbS/CdS, PbS/Mn-CdS. The PbS/Mn-CdS photo-anode has the highest charge transfer resistance R_{ct} (40.04 Ω) among the other electrodes and the highest chemical capacitance Cμ (3954 μF), indicating more rapid charge transport at the TiO_2/electrolyte/QD interface. The relatively high values of R_{CT} and Cμ (PbS/Mn-CdS) yields the excellent value of lifetime of which contributes to keep V_{OC} at a high level by avoiding electron loss in the semiconductor. The bare CdS has lower R_{CT} (6.19 Ω) and the lowest Cμ (1399 μF) because of the much lower electron transfer at the TiO_2/QDs/electrolyte interface. [49]

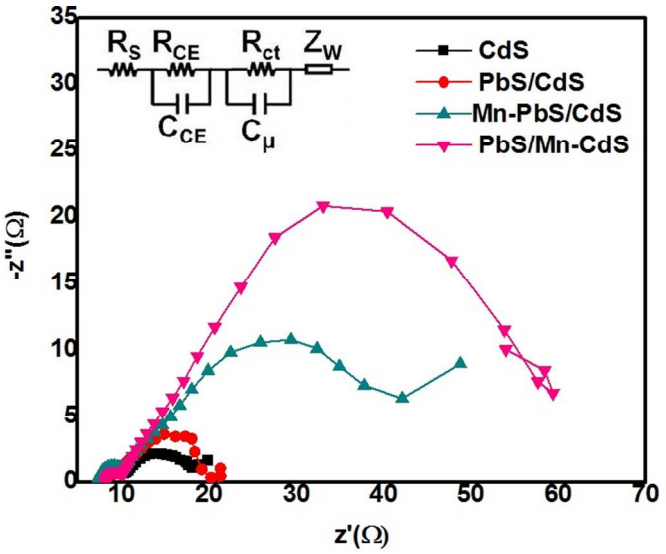

Figure 9.EIS spectra of QDSSCs based on CdS, PbS/CdS, Mn-PbS/CdS and PbS/Mn-CdS electrodes measured at the frequency range 100 mHz–500 kHz.

Table 3 Summary of the photovoltaic properties and EIS results of CdS, PbS/CdS, Mn-PbS/CdS and PbS/Mn-CdS electrodes with CuS counter electrode.

Parameter	CdS	PbS/CdS	Mn - PbS/CdS	PbS/Mn - CdS
Rs (Ω)	9.24	9.61	8.29	8.32
R_{CE}(Ω)	5.01	6.33	5.39	4.04
Rct(Ω)	6.19	7.35	30.05	40.04
Cμ(μF)	1399	3899	3887	3954
Z_d(Ω)	0.99	1.29	5.54	8.11

The Mn leads to an increased electron transfer rate and improved efficiency of the solar cells. The increase in the R_{ct} on PbS/Mn- CdS is with the Mn ions on CdS leads to higher resistance of the photo-anode. The reduced Cμ indicates lower electron density due to the absence of Mn ions. The higher Z_d is because of the thicker porous of PbS/Mn-CdS materials increased the diffusion length.

The Bode phase plots for cells with different configurations are shown in Figure 10.The electron life times (τ_r) can be obtained according to the following equation:

$$\tau_r = 1/(2\pi f_{max}), \quad (1)$$

where f_{max} is the maximum frequency of the middle-frequency peak in the Bode plot. The τ_r values of CdS, PbS/CdS, Mn-PbS/CdS, PbS/Mn-CdS. were found to be 24.36, 30.74, 50.8 and 47.2ms, respectively. The higher τ_r value of the PbS/Mn-CdS suggests that electrons have a longer lifetime and are effectively transferred, resulting in higher J_{SC} and energy conversion efficiency for the QDSSCS. The frequency peak of PbS/Mn-CdS shifted to lower frequency, which is ascribed to the enhanced electron transport. Electrons with higher mobility can travel a longer distance with fewer surface traps.

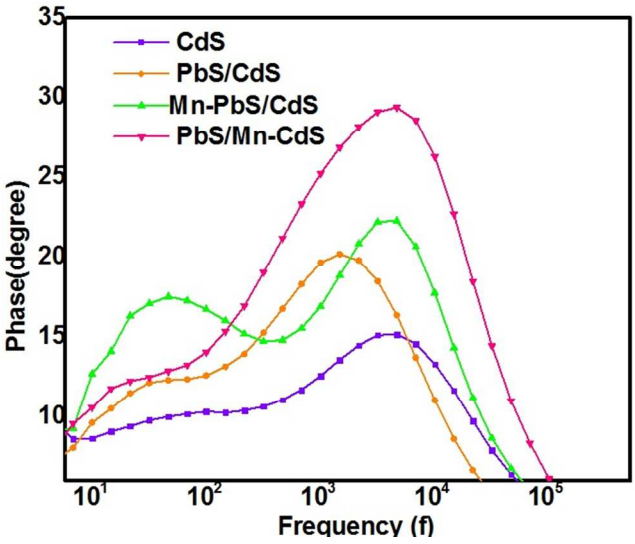

Figure 10. Bode plots of QDSSCs based on CdS, PbS/CdS, Mn-PbS/CdS and PbS/Mn-CdS electrodes measured at 0.6 V bias potential in the frequency range 100 mHz–500 kHz.

3.5 Stability

Cell device stability is often overlooked, but it is crucial to any real application. The stability of the working state of CdS, PbS/CdS, Mn-PbS/CdS and PbS/Mn-CdS photo-anodes of QDSSCs with the CuS CE was measured in our work. Figure 11 shows a comparison of the extracted photovoltaic parameters (Voc, η ,Jsc and FF) of the CdS, PbS/CdS , Mn-PbS/CdS and PbS/Mn-CdS curves from stability tests for nearly 10 h. The devices were stored in air with ambient light illumination and without further encapsulation.

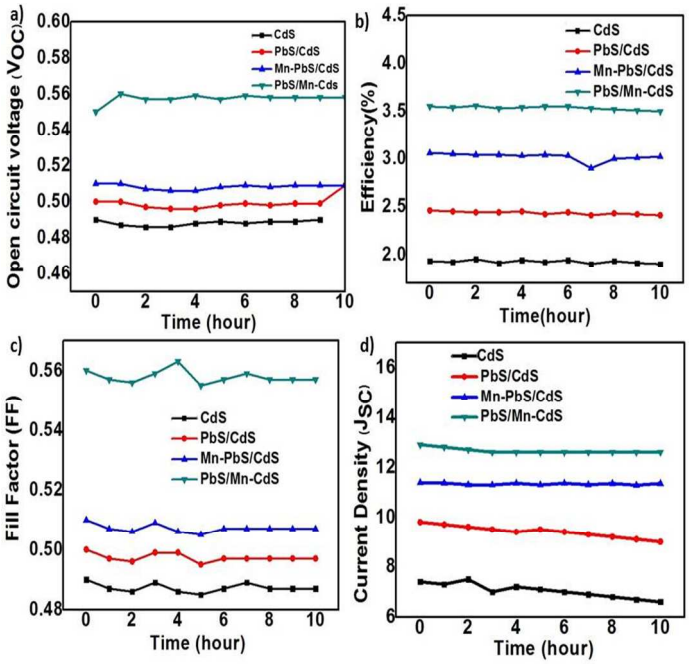

Figure 11. Stability test: Evolution of photovoltaic parameters values, (a) Voc, (b) Efficiency (η), (c) FF, and (d) J_{SC} for the QDSSC based on CdS, PbS/CdS, Mn-PbS/CdS and PbS/Mn-CdS electrodes.

The η values of the CdS photo-anode declined continuously from 1.93% to 1.69% within 10 h, the PbS/CdS values maintained stabled, Mn-PbS/CdS values started to decrease from 3.06 to 2.8% whereas the power conversion efficiency values of the PbS/ Mn-CdS photo-anode decreased in the first 2 h from 3.55% to 3.3%, but excellent constant η values were maintained thereafter. The mid gap states created by Mn doping cause electrons to get trapped and screen them form charge recombination with holes and oxidized polysulfide electrolyte. Therefore, the spatial separation of electrons can be efficiently collected using an external circuit. In Mn-CdS, the enhanced photo-stability could be attributed to efficient holes scavenging capability of polysulfide electrolyte, which successfully

suppresses hole-induced anodic corrosion. The reduced recombination could be improving the photo-stability of the QDSSCs.

The PCE improvement is likely derived from two factors: reduced recombination losses due to the combination of Mn and PbS passivation. A more complete passivation of QD surfaces is also a likely reason for the improved device stability. We have demonstrated high-performance QDSSCS through engineering of the band alignment at the QDs and the QDs/anode interface. These solar cells were processed in air at room temperature and exhibit excellent stability. We expect that determining the origin of the high V_{OC} and the combinations of Mn with PbS and CdS QDs distinctly will result in continued efficiency improvements. Greater understanding of the QD optoelectronic properties and further progress in materials development could lead to the generation of much more stable QDSSCs with higher efficiency.

4 Conclusions

In summary, we have fabricated lead PbS/Mn-CdS quantum dots on the surface of TiO_2 by simple successive ion layer adsorption and reaction method. We obtained a comparison between CdS, PbS/CdS, Mn-PbS/CdS and Mn-doped CdS photo-anodes, which revealed that the PbS/Mn-CdS can be considered as an alternative photo-anode to CdS PbS/CdS, Mn-PbS/CdS in many applications, owing to its faster charge transport, more efficient charge separation, recombination resistance, and greater stability. A maximum 12.9 mA cm^{-2} current density and 3.55% conversion efficiency under one sun illumination has been achieved by doping of Mn in CdS and the quantum dot sensitised solar cell (QDSSC) performance is enhanced which is attributed due to the better light harvesting ability of PbS quantum dots and makes large accumulation of photo-injected electrons in the conduction band of TiO_2. The doping of CdS films with Mn has enabled us to achieve improvement in the power conversion efficiency as compared to CdS, PbS/CdS, Mn-PbS/CdS .This result confirms that the Mn ions on the CdS was very effective for improving the surface properties regarding both chemical stability and electronic surface state by reinforcing the surface network in QDSSC compared with Mn-PbS/CdS. We believe that the QDSSC with efficiency exceeding 6% can be achieved with the co-sensitization of longer absorption wavelength materials such as CdSe or PbS on the surface of PbS/Mn-doped CdS with ZnS passivation layer. Future work will be devoted to a systematic study of the role of quantum confinement on tuning the exchange interactions.

Acknowledgements

This research is supported by Basic Science Research Program through the National Research Foundation of Korea (NRF) funded by the Ministry of Education, Science and Technology (2011-0014437).

Notes and references

[a] Department of Electrical and Computer Engineering, Pusan National University, Gumjeong-Gu, Jangjeong-Dong, Busan609-735, South Korea

[b] Department of Physics, Pusan National University, Gumjeong-Gu, Jangjeong-Dong, Busan 609-735, South Korea

[c] Department of Computer Engineering, Pusan National University, Gumjeong-Gu, Jangjeong-Dong, Busan609-735, South Korea,

References

1 A. L. Rogach, Semiconductor nanocrystal quantum dots, Wien, New York, Springer, 2010, **ISBN 978-3-211-99913-4.**

2 G. D. Scholes, G. Rumbles, *Nature Materials,* 2006, **5**,683.

3 J.Y. Kim, O. Voznyy, D. Zhitomirsky, E. H.Sargent, *Advanced Material*, 2013, **25**, 4986.

4 S. A. Wolf, D. D. Awschalom, R. A. Buhrman, J. M. Daughton, S. von Molnar, M. L. Roukes, A. Y. Chtchel kanova, D. M. Treger, *Science*, 2001, **294**,148.

5 A. Babinski, M. Potemski and P. C. M. Christianen, *Comptes Rendus Physique*, 2013, **14,** 121.

6 R. J. Ellingson, M. C. Beard, J. C. Johnson, P. R. Yu,O. I. Micic, A. J. Nozik, A. Shabaev and A. L. Efros, *Nano Letters,* 2005, **5** ,865.

7 G. Nair, L. Y. Chang, S. M. Geyer and M. G. Bawendi, *Nano Letters*, 2011, **11**,2145.

8 A. J. Nozik, M. C. Beard, J. M. Luther, M. Law, R. J. Ellingson and J. C. Johnson, *Chemical Reviews,* 2010, **110**, 6873.

9 Rowley, J. G. Farnum, B. H. Ardo, S. Meyer, *Journal of physical chemistry letters*, 2010, **1**,3132.

10 Call. F, Stolwijk, N. A, J*ournal of physical chemistry letters,* 2010, **1**,2088.

11 Chandu V. V. M. Gopi, M. Venkata-Haritha, Soo-Kyoung Kim, Hee-Je Kim, *Dalton Transactions,* 2015, **44**,630.

12 X. Z. Lan, J. Bai, S. Masala, S. M. Thon, Y. Ren, I. J. Kramer, S. Hoogland, A. Simchi, G. I. Koleilat, D. Paz-Soldan, Z. J. Ning, A. J. Labelle, J. Y. Kim, G. Jabbour and E. H. Sargent, *Advanced materials*, 2013, **25**, 1769.

13 C. Piliego, L. Protesescu, S. Z. Bisri, M. V. Kovalenko M. A. Loi, *Energy and environmental science,* 2013, **6**,3054.

14 N. Guijarro, J. M. Campina, Q. Shen, T. Toyoda, T. Lana Villarreal, R. Gomez, *Physical chemistry chemistry physics*, 2011, **13**,12024.

15 R. Trevisan, P. Rodenas, V. Gonzalez-Pedro, C. Sima, R. S. Sanchez, E. M. Barea, I. Mora-Sero, F. Fabregat-Santiago and S. Gimenez, *Journal of physical letters*, 2013, **4**, 141.

16 Z. X. Pan, H. Zhang, K. Cheng, Y. M. Hou, J. L. Hua and X. H. Zhong, *ACS Nano*, 2012, **6** ,3982.

17 S. Kruger, S. G. Hickey, S. Tscharntke and A. Eychmuller, *Journal of physical chemistry C*, 2011, **115**, 13047.

18 S. Hachiya, Q. Shen and T. Toyoda, *Journal of applied physics,* 2012, **111**, 104315.

19 Y.L. Lee and Y.S. Lo, *Advanced functional materials*, 2009, **19**, 604.

20 Z. Tachan, M. Shalom, I. Hod, S. Ruhle, S. Tirosh, *Journal of physical chemistry C*, 2011, **115**, 6162.

21 A. Salant, M. Shalom, Z. Tachan, S. Buhbut, A. Zaban and U. Banin, *Nano Letters,* 2012, **12**, 2095.

22 I. Robel, V. Subramanian, M. Kuno and P. V. Kamat, *Journal of American chemical society*, 2006,**128**,2385.

23 I. Mora-Sero, S. Gimenez, F. Fabregat-Santiago, R. Gomez, Q. Shen, T. Toyoda, J. Bisquert, *Accounts of chemical research,* 2009,**42,**1848.

24 T. Toyoda, K. Oshikane, D. Li, Y. Luo, Q. Meng, Q. Shen, *Journal of applied physics*, 2010,**108**,114304.

25 L. J. Diguna, Q. Shen, J. Kobayashi, T. Toyoda, *Applied physical letters,* 2007,**91**, 023116.

26 Y.-L. Lee and C.-H.Chang, *Journal of Power Sources,* 2008, **185**,584.

27 D. R. Baker,P. V. Kamat, *Advanced functional materials*, 2009, **19** ,805.

28 S. S. Mali, S. K. Desai, S. S. Kalagi, C. A. Betty, P. N. Bhosale R. S. Devan, Y. R. Ma and P. S. Patil, *Dalton transactions,* 2012, **41**, 6130.

29 M. Jones, S. S. Lo and G. D. Scholes, *Proceedings of the National Academy of Sciences, U.S.A.,* 2009, **106**, 3011.

30 A. H. Ip, S. M. Thon, S. Hoogland, O. Voznyy, D. Zhitomirsky, R. Debnath, L. Levina, L. R. Rollny, G. H. Carey, A. Fischer, K. W. Kemp, I. J. Kramer, Z. Ning,A. J. Labelle, K. W. Chou, A. Amassia E. H. Sargent, *Nature nanotechnology,* 2012,**7**, 577.

31 M. V. Kovalenko, R. D. Schaller, D. Jarzab, M. A. Loi and D. V. Talapin, *Journal of American society,* 2012,**134,** 2457.

32 S.M. Yang, C.H. Huang, J. Zhai, Z.S. Wang and L. Jiang, *Journal of material chemistry,* 2002,**12**,1459.

33 S. Buhbut, S. Itzhakov, D. Oron, A. Zaban, *Journal of physical chemistry letters,* 2011**, 2,** 1917.

34 H.Y. Fu, S.W. Tsang, Y.G. Zhang, J.Y. Ouyang, J.P. Lu, K. Yu, Y. Tao, *Chemistry of materials,* 2011, **23,**1805.

35 V. Chikan, Journal of physical chemistry letters, 2011, **2**, 2783.

36 Lyudmila Turyanska , Fabrizio Moro , Andrew N. Knott , Michael W. Fay , Tracey D. Bradshaw , and Amalia Patane, P*article & Particle Systems Characterization*, 2013, **30**, 945.

37 G Long, B Barman, S Delikanli1, Y Tsung Tsai1, P Zhang, A Petrou1 and H Zeng, *Applied physics letters,* 2012, **101** ,062410.

38 C. Justin Raj, S.N. Karthick, Songyi Park , K.V. Hemalatha, Soo-Kyoung Kim , K. Prabakar , Hee-Je Kim, *Journal of Power Sources*, 2014, **248**, 439.

39 P.K. Santra, P.V. Kamat, *Journal of American chemical society,* 2012, **134,** 2508.

40 L.Yu, Z. Li, Y. Liu, F. Cheng, S. Sun, *Applied Surface Science,* 2014, **309**, 262.

41 S. Srinivasa Rao, Chandu. V.V.M. Gopi, Soo-Kyoung Kim, Min-Kyu Son, Myeong-Soo Jeong, A.Dennyson Savariraj, K. Prabakar, Hee-Je Kim, *Electrochimica Acta,* 2014,**133**, 174.

42 I Lim , D Yoon Lee, S. A. Patil , N. K. Shrestha a, S Hyung Kang ,Yoon-Chae Nah , W Lee ,Sung-Hwan Han, *Materials Chemistry and Physics,* 2014,**148**,562.

43 Y. Al-Douri, Q. Khasawneh, S. Kiwan, U. Hashim, S.B. Abd Hamid, A.H. Reshak, A. Bouhemadou, M. Ameri, R. Khenata, *Energy conversion and management*, 2014, **82,** 238.

44 A. Braga, S. Gimenez, I. Concina, A. Vomiero, I.M. Sero, *Journal of physical chemistry letters,* 2011**, 2 ,**454.

45 H. Lee, H.C. Leventis, S.J. Moon, P. Chen, S. Ito, S.A. Haque, T. Torres, F. Neuesch,T. Geiger, S.M. Zakeeruddin, M. Gratzel, M. Nazeerruddin, *Advanced functional materials*, 2009**, 19,** 2735.

46 I. Robel, M. Kuno, P.V. Kamat, *Journal of American chemical society,* 2007, **129,** 4136.

47 J. Jiao, Z.J. Zhou, W.H. Zhou, S.X. Wu, 2013, **16,** 435.

48 K.M. Lee, V. Suryanarayanan, K.C. Ho, Solar energy materials and solar cells, 2007, **91,** 1416-1420.

49 W.Q. Wu, B.X. Lei, H.S. Rao, Y.F. Xu, Y.F. Wang, C.Y. Su, D.B. Kuang, 2013, **3,** 1352.

Table of Contents (TOC)

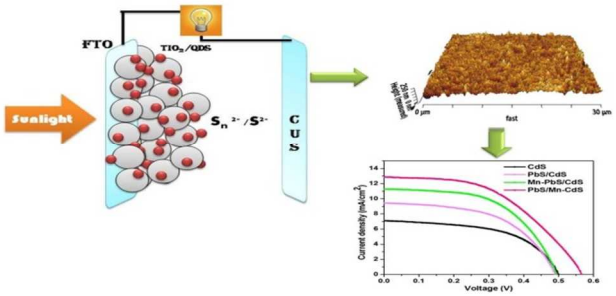

The PbS/Mn-CdS electrode shows superior stability in sulfide/polysulfide electrolyte with power conversion efficiency (η) of 3.55%.